npj | materials degradation

Brief communication

Published in partnership with CSCP and USTB

https://doi.org/10.1038/s41529-024-00485-3

Polymerised forms in the zirconium conversion coatings on cold-rolled steel: proof of concept

Check for updates

Ana Kraš[1,2], Ingrid Milošev[1], Antoine Seyeux[3] & Philippe Marcus[3]

This study validates the proposed polymerised structure, including tetrameric polynuclear species, of solid amorphous oxyhydroxide zirconium conversion coatings on cold-rolled steel using ToF-SIMS. Tetramers are formed at pH near 4 (and possibly higher), with thickness increasing over extended conversion times. EIS in simulated acid rain further demonstrates that optimal coating formation requires a pH of at least 4 and a sufficient conversion time for adequate thickness, confirmed by the high-frequency EIS loop. Tetramer forms were not observed when the coatings were prepared at lower pH or shorter conversion time, proving that the polymerisation step is crucial for obtaining the coatings offering adequate corrosion protection.

Being a commercially viable substitute for chromate and phosphate conversion coatings, a comprehensive understanding of zirconium aqueous chemistry is essential for maximising the practical applications of zirconium conversion coatings (ZrCCs), as shown in our previous work[1]. However, the investigation of zirconium aqueous chemistry is significantly hindered by its extensive hydrolysis, resulting in the concurrent existence of many monomeric and polymeric species in the solution. Fast exchange of geometry and coordination further complicates the study, making it highly sensitive to solution starting conditions, especially ageing, pH, concentration, and complexing agents[2,3].

Our recent review of existing thermodynamic data and formulated equilibrium diagrams for Zr−OH and Zr−F systems has shed light on ZrCCs containing Zr in a tetrameric form within the amorphous oxide phase at ZrCC bath operating conditions, otherwise mirroring the proposed structure suggested some time ago by Clearfield[4].

Advancements in comprehending the polymerisation paths and species involved in Zr−OH systems have been achieved by applying sophisticated scattering, absorption, and resonance spectroscopy methods coupled with computer simulations[5–11]. To our knowledge, no experimental studies have focused on the speciation of polymeric species in Zr−F solutions related to zirconium conversion baths. The formation of polymeric Zr species is, unfortunately, further impeded by the complexation with fluorides, given that most conventional ZrCC baths rely on H_2ZrF_6 solutions.

To experimentally validate the proposed concept involving the tetrameric Zr as the main building block of the precipitating ZrCC, in this study, we employed a more accessible technique—time-of-flight secondary ion mass spectrometry (ToF-SIMS)—to investigate ZrCCs prepared at selected bath operating conditions on a cold-rolled steel substrate. So far, ToF-SIMS has been used to investigate zirconium oxide distribution in conversion layers produced by trivalent chromium process (TCP)[12–14]. Recognised for its exceptional surface sensitivity, ToF-SIMS provides structural insights based on mass fragments, thus being able to identify polymeric Zr species[15–17].

Results and discussion

ToF-SIMS results

Three different ZrCC bath parameter combinations were employed, determined through response surface methodology (RSM) in our forthcoming work[18]. At bath concentration of 825 ppm H_2ZrF_6, ZrCCs were prepared at two conversion times (60 and 480 s) and pH values (3 and 4): (i) pH of 3 leads to inadequate coating formation, (ii) pH of 4 with 60 s conversion time leads to a very thin, non-corrosion-resistant coating, and (iii) pH of 4 with 480 s conversion time results in a thicker coating, exhibiting improved corrosion resistance compared to bare samples.

Figure 1 depicts overlapped mass spectra in the m/z range 0−540 measured on ZrCCs prepared on cold rolled steel at the three combinations of bath parameters (pH of 3 (red), pH of 4 with 60 s (blue) and 480 s (grey) conversion time). A peak selection encompassing monomeric (120−160), dimeric (240−290), trimeric (380−420), and tetrameric (500−540) Zr fragments of the type $Zr_nO_m(OH)_p^-$ is also indicated in Fig. 1. More precisely, high-intensity mass peaks are evident in the 380−400, 400−420, 500−520, and 520−540 mass ranges (m/z) for coatings prepared at a pH 4. This observation implies that polymerised ZrCC layers form at a pH of 4 and possibly at a higher pH, supporting the results from our forthcoming work[18].

[1]Jožef Stefan Institute, Department of Physical and Organic Chemistry, Jamova c. 39, Ljubljana 1000, Slovenia. [2]Jožef Stefan International Postgraduate School, Jamova c. 39, Ljubljana 1000, Slovenia. [3]CNRS – Chimie ParisTech, Institut de Recherche de Chimie Paris, Physical Chemistry of Surfaces Group, 11 rue Pierre et Marie Curie, Paris 75005, France. e-mail: ingrid.milosev@ijs.si; philippe.marcus@chimieparistech.psl.eu

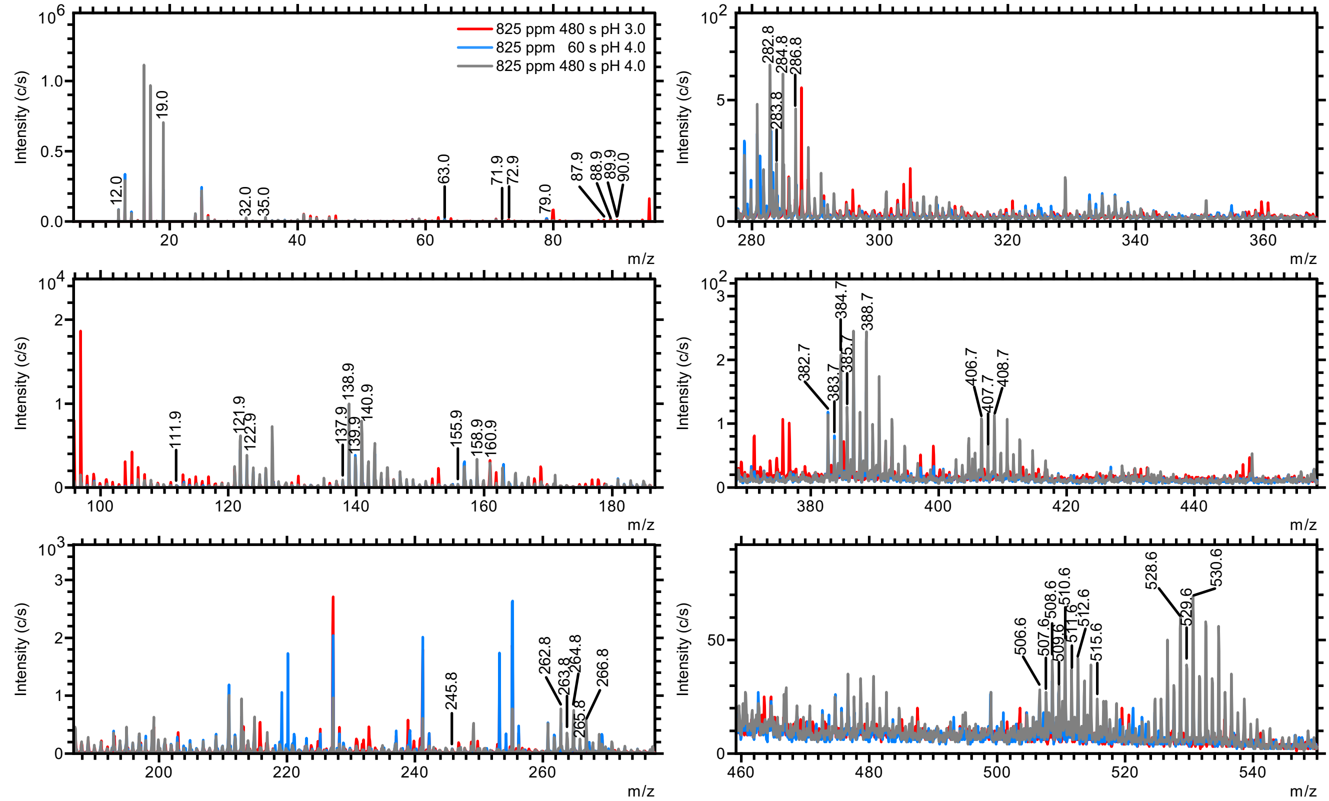

Fig. 1 | Mass spectra (negative polarity) in the *m/z* range 0−540 measured on ZrCCs prepared on cold rolled steel at three combinations of bath parameters as indicated in the legend. Characteristic ion fragments are presented in Supplementary Table 1.

A comprehensive list of negative ion fragments obtained in the 0−540 m/z mass range, along with their corresponding masses, is presented in Supplementary Table 1, with selected high-resolution ToF-SIMS mass spectra in Fig. 2.

Supplementary Table 1 additionally provides information on the potential existence of $Zr_nO_m(OH)_pF_q^-$ along with certain specific $Zr_nO_m(OH)_p^-$ species, as fluoride is demonstrated to incorporate into ZrCCs in the form of oxyfluorides[19,20]. We believe the most likely mechanism involves the isomorphic substitution of F^- with OH^- during the hydroxylation of ZrF_6^{2-}, resulting in the formation of aquahydroxo/aquafluorohydroxo complexes, leading to condensation and, ultimately, precipitation[1].

The ToF-SIMS depth profiles of $Zr_nO_mH_p^-$ and $Zr_nO_mH_pF_q^-$ species are presented in Fig. 3. Please note that a more precise record would be $Zr_nO_m(OH)_p^-$ and $Zr_nO_m(OH)_pF_q^-$. However, since ToF-SIMS cannot differentiate between oxygen originating from oxide or hydroxide, we opted for a more simple record $Zr_nO_mH_p^-$ and $Zr_nO_mH_pF_q^-$. Zr species in Fig. 3 were selected based on the highest signals observed in the sample at 825 ppm/480 s/ pH 4, further reflecting the results in Figs. 1 and 2. The Fe_2^- signal originating from the metallic substrate is also added since it allows the ZrCC/substrate interface to be positioned (vertical line in Fig. 3). Evidently, as the conversion time and pH increase, the thickness of the ZrCC increases, following this trend: 250 s for the sample 825 ppm/480 s/pH 3, 820 s for 825 ppm/60 s/pH 4, and 1800 s for 825 ppm/480 s/pH 4, that corresponds to 5, 16.5, and 36 nm, respectively (assuming a constant sputtering rate of 0.02 nm/s, estimated from previous work on a TCP conversion coating[12]). Looking deeper at the ZrCC layer, it can be observed that the maximum intensities of all Zr-containing species increase from pH 3 to pH 4, suggesting that the ZrCC, in addition to being of low thickness, does not fully cover the substrate at pH 3. Additionally, the intensities of Zr peaks decrease from monomeric to tetrameric species, likely due to fragmentation. The primary Zr peak observed is ZrO_2^-, consistent with similar previous ToF-SIMS studies at lower *m/z*[21]. The Fe_2^- signal, associated with the metallic substrate, exhibits a steeper increase with sputtering time for the coating prepared at shorter conversion times and lower pH. This suggests the broadening of the ZrCC/substrate interface, presumably due to the increased roughness with the ZrCC layer thickness. Additionally, detecting FeO_2^- (and $FeOOH^-$, results not shown in the figure) signals between the substrate and ZrCC suggests the presence of an intermediate layer of ferrous oxide/hydroxide at the interface, likely resulting from the alkaline cleaning step.

The tetrameric structure proposed by Clearfield for amorphous zirconia[4], as applied to ZrCCs in our previous study[1], is identified as $Zr_4(OH)_8^{8+}$, with the possibility of higher polynuclear forms and less charged species[8]. However, ToF-SIMS measurements do not allow the exact ionic hydration structure to be deducted. Thus, our primary objective was to identify polymeric fragments and, most importantly, to confirm tetrameric ones, as their higher kinetic stability, facilitated through cyclisation, is the most probable cause for their incorporation from solution to precipitate[1]. Although not measured in the solution, ToF-SIMS allows us to infer a plausible connection between the aqueous species involved in the solid-phase formation in the precipitate and confirm the proposed structure of ZrCCs. The tetrameric peak, although not the most intensive among polymeric species (Fig. 3), can undoubtedly confirm that ZrCC contains Zr in the tetrameric form, considering its fragmentations during ToF-SIMS measurements. Finally, and most notably, trimeric and tetrameric structures are present in samples obtained at higher pH, strongly suggesting that not only does the ZrCC thickness increase with longer conversion times but also that polymerised coating forms at pH near 4. Also, the intensities of Zr peaks in the case of pH = 3 are very low, suggesting that almost no conversion layer is formed at pH of 3 (*vide infra*).

EIS results

The EIS results (Supplementary Table 2) obtained for the chosen ZrCC bath parameter combinations, albeit in a slightly more acidic medium of simulated acid rain (pH ≈ 5) (Fig. 4), show similar Nyquist plot shapes for the

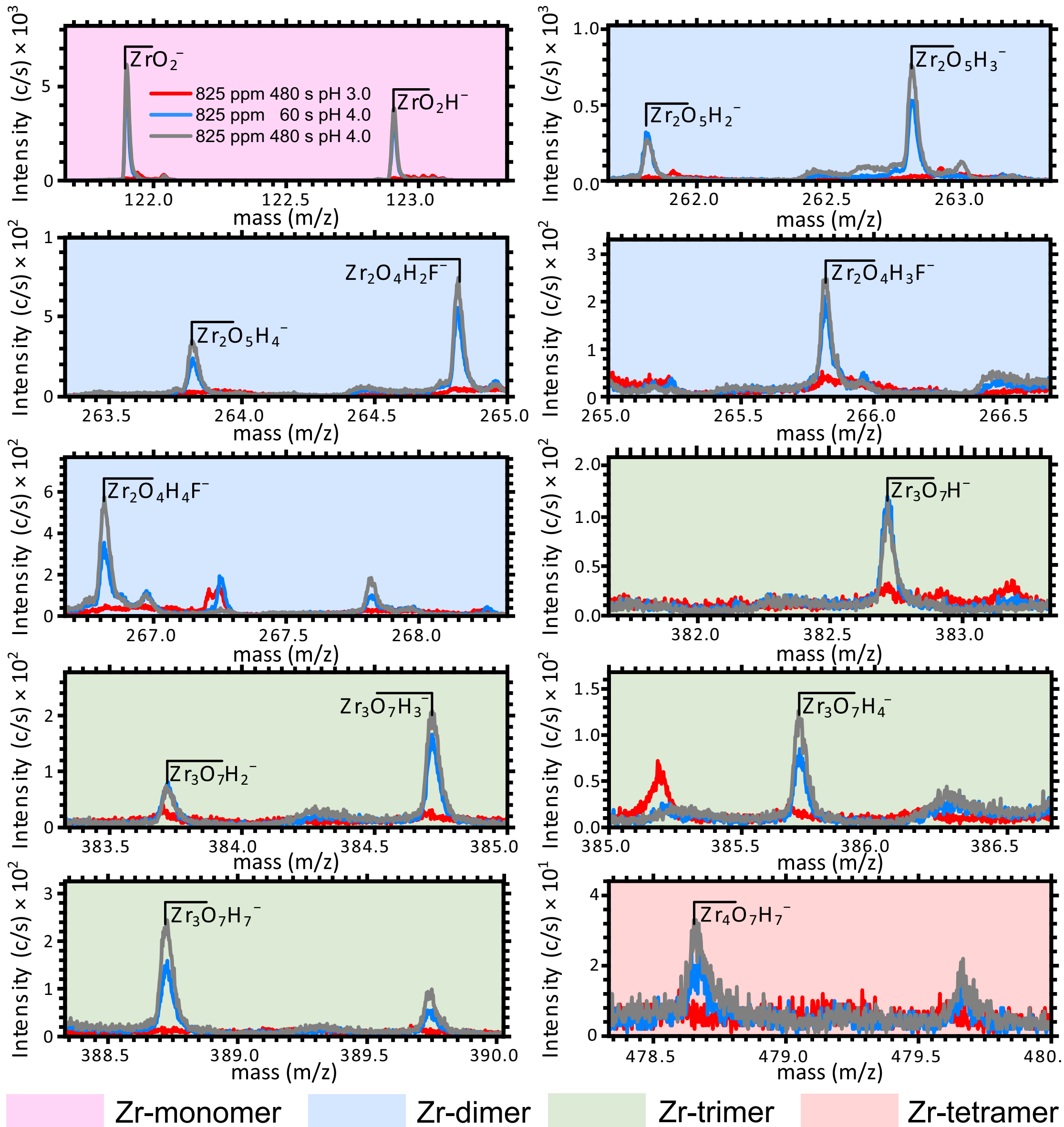

Fig. 2 | ToF-SIMS negative ion spectra of ZrCCs prepared at various combinations of bath parameters on cold rolled steel. Characteristic fragmentation ions are assigned.

samples prepared in the same manner in dilute Harrison's solution (pH = 5.2)[18]. The EIS fitting procedure and discussion, thoroughly elaborated in that work[18], can be seamlessly applied herein. Equivalent electrical circuits (EECs) used for fitting are given in Fig. 4a and b. It can be seen that samples exhibited either one (Fig. 4a) or three time (Fig. 4b) constants. R_e refers to the electrolyte resistance. The first unresolved high-frequency time constant (R_{po}—CPE_{cc}), with a small capacitive loop deemed negligible due to effects from the reference electrode, can be attributed to the electrolyte resistance inside pores at the passive film/electrolyte interface (R_{po}) or possibly to the dielectric properties of the barrier surface film, namely, the zirconium conversion coating (CPE_{cc})[22]. Therefore, in cases with three time constants, an EEC including only two time constants was utilised (Fig. 4b), with the sum of the latter two time constants giving the value of the overall polarisation resistance (R_p)[18]. The second, middle-frequency time constant (R_{ct}—CPE_{dl}) is related to the charge transfer resistance (R_{ct}) within defects and the CPE_{dl} to a double-layer capacitance[23]. The third, low-frequency time constant (R_{cp}—CPE_{cp}), not fully resolved due to a limited number of measurements, is associated with the capacitive behaviour of corrosion products (CPE_{cp}), with R_{cp} indicating the relaxation of these products on the electrode surface[23–28]. A detailed EIS and scanning electron microscopy analysis to be provided in our forthcoming work[18] will discuss the high-frequency loop observed only in the sample at 825 ppm/pH 4/480 s, indicative of adequate ZrCC formation (Fig. 4c), in contrast to the EEC with a single time constant, where all other time constants merge into R_{ct}—CPE_{dl} (Fig. 4a) seen in the bare sample and those with inadequate coating—either too thin at 825 ppm/pH 4/60 s or absent, with ZrCC nodules at 825 ppm/pH 3/480 s—reflected in lower R_p values. Bode plots are provided in Supplementary Fig. 1. It is evident that the sample treated for 480 s at pH 4.0 offers superior corrosion resistance in terms of both phase angle and impedance modulus.

Summarising, EIS and ToF-SIMS results suggest that adequate ZrCCs are those that are polymerised, contain a tetrameric structure and are obtained at longer conversion times. Using ToF-SIMS, the presence of polymerised film, including tetrameric species, in ZrCCs was confirmed. Evidently, ToF-SIMS showed that tetrameric structures are identified in ZrCCs prepared at a pH of 4, increasing with longer conversion times. This is further confirmed by EIS data in simulated acid rain, suggesting that adequate ZrCC formation requires at least a pH of 4 (and possibly, higher)

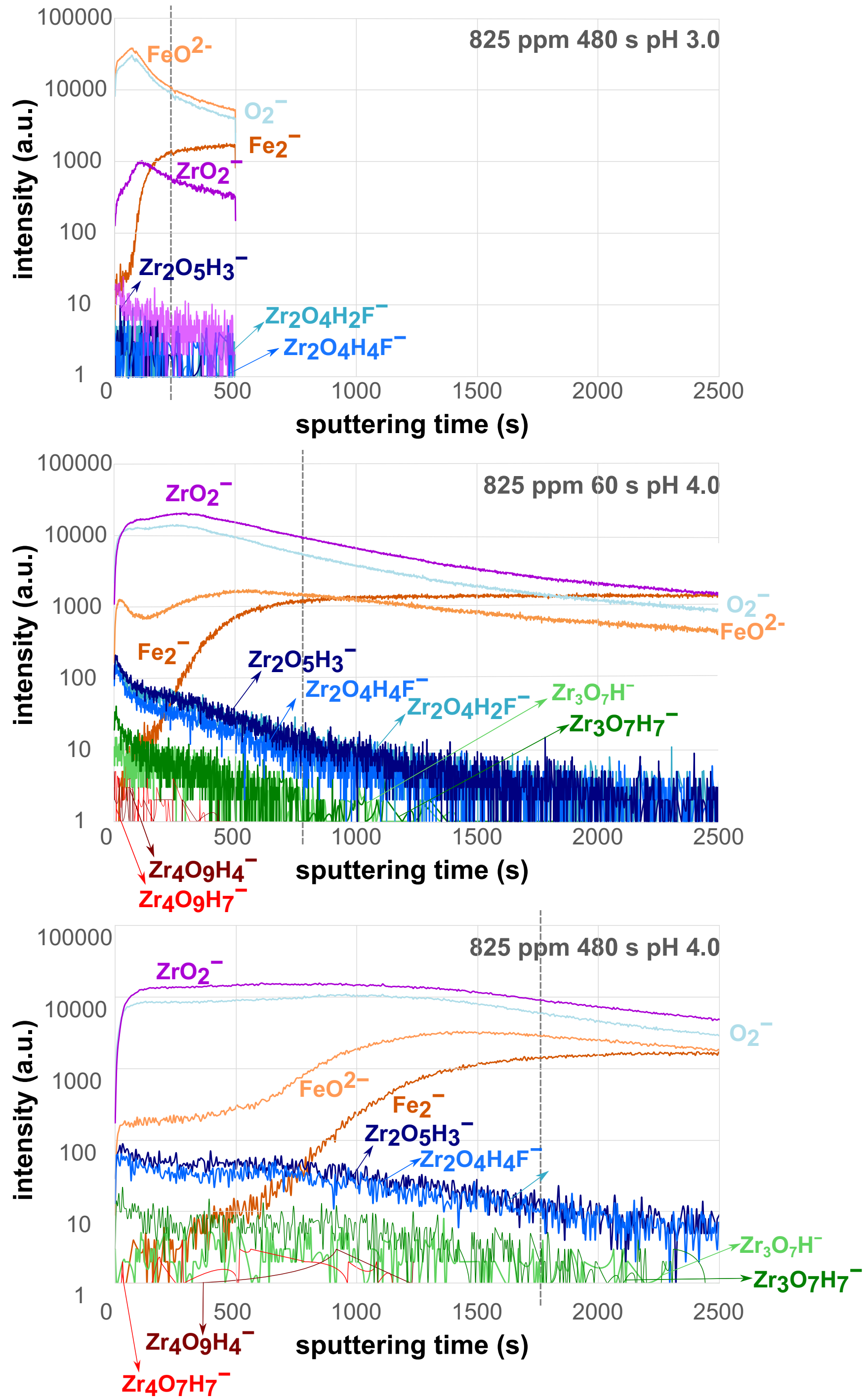

Fig. 3 | ToF-SIMS depth profiles of selected Zr and Fe fragments of ZrCCs prepared using three combinations of bath parameters. Grey dashed vertical lines indicate the ZrCC thickness obtained from the drop of the oxygen intensity peak value to half.

and a sufficient conversion time (480 s herein) for the desired thickness. The thickness adequacy is affirmed by a high-frequency EIS loop, emphasising the significance of specific pH and conversion time conditions for effective ZrCC formation. Nevertheless, understanding the hydration numbers of ions, rates of exchange of coordinated water molecules around ions, and interaction energies between ions and water molecules requires advanced scattering methods. Therefore, fully unravelling the ZrCC formation mechanism awaits future research work.

Methods

All additional experimental details considering sample preparation, chemicals, ToF-SIMS and EIS measurements are provided in the Supplementary material. Furthermore, Supplementary Fig. 2 concisely illustrates the experimental flow. More comprehensive information will be given in our forthcoming work[18].

Samples

Low-carbon cold-rolled steel (CRS) was sourced as a 1 mm-thick panel from ACT Test Panels LLC in Hillsdale, MI, USA, having the following chemical composition obtained by X-ray fluorescence spectroscopy: C 0.04, Mn 0.2, S 0.01 wt%, Fe remaining. The panel was cut into smaller 2.5 cm × 3.5 cm sheet specimens with 3 mm diameter holes punched for easier immersion into H_2ZrF_6 conversion bath solutions and subjected to electrochemical impedance spectroscopy (EIS) measurements. For ToF-SIMS analysis, the panel

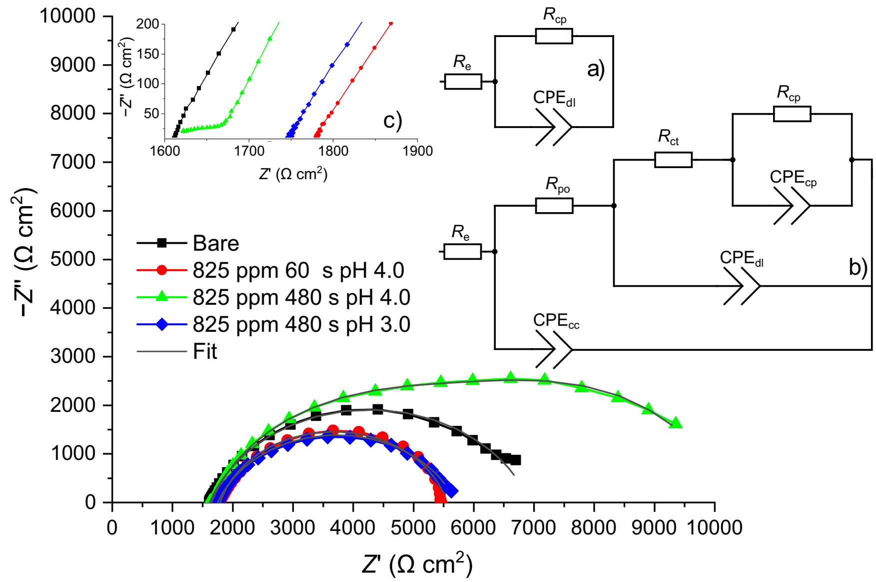

Fig. 4 | EIS spectra measured in simulated acid rain (pH ≈ 5) on ZrCCs prepared on cold-rolled steel at three combinations of bath parameters. The enclosed EECs **a**, **b** were utilised for fitting. Only EEC in **b** was applied on 825 ppm/480 s/pH 4. Although EEC has three time constants, the R_{po}−CPE_{cc} component was not utilised for fitting; the sum of the latter two time constants gave the value of the overall polarisation resistance (R_p); more details are given in the text. The remaining samples were fitted with EEC in (**a**). The inset **c** displays high-frequency spectra. Bode plots are provided in Supplementary Fig. 1.

was cut to dimensions ≤1 cm². Before conversion treatment, samples were mechanically ground and pretreated chemically (Supplementary Fig. 2).

ToF-SIMS

ToF-SIMS analysis was conducted using a ToF-SIMS 5 spectrometer (IonTof—Münster, Germany) under a base pressure of 5×10^{-9} mbar. The data acquisition and post-processing analysis were performed using SurfaceLab software v7. The spectrometer was run in high current (HC) bunched mode with a high mass resolution (DM/M around 7000, measured on Si peak). The exact mass values of at least five known species were used to calibrate the data acquired in the negative ion polarity. All samples were cleaned before introduction into the spectrometer.

EIS

EIS measurements were performed in homemade modified "clamp-on" electrochemical cells (250 mL). A three-compartment setup included the sample as the working electrode (WE), a carbon rod as the counter electrode (CE), and a saturated Ag/AgCl (3 M) electrode as the reference electrode (E = 0.297 V vs. standard hydrogen electrode). The WE area was 0.785 cm², and measurements were conducted under ambient conditions. The electrolyte used was simulated acid rain, pH ≈ 5. More details on the experimental data can be found in the Supplementary material.

Data availability

The authors declare that all data supporting the findings of this study will be made available upon request.

Received: 19 March 2024; Accepted: 31 May 2024;
Published online: 18 June 2024

References

1. Kraš, A. & Milošev, I. The aqueous chemistry of zirconium as a basis for better understanding the formation of zirconium conversion coatings: updated thermodynamic data. *J. Electrochem. Soc.* **170**, 21508 (2023).
2. Connick, R. E. & McVey, W. H. The aqueous chemistry of zirconium. *J. Am. Chem. Soc.* **71**, 3182–3191 (1949).
3. Macdermott, T. E. The structural chemistry of zirconium compounds. *Coord. Chem. Rev.* **11**, 1–20 (1973).
4. Clearfield, A. Structural aspects of zirconium chemistry. *Rev. Pure Appl. Chem.* **14**, 91 (1964).
5. Southon, P. D., Bartlett, J. R., Woolfrey, J. L. & Ben-Nissan, B. Formation and characterization of an aqueous zirconium hydroxide colloid. *Chem. Mater.* **14**, 4313–4319 (2002).
6. Rao, N., Holerca, M. N. & Pophristic, V. Computational study of the small Zr(IV) polynuclear species. *J. Chem. Theory Comput.* **4**, 145–155 (2008).
7. Hagfeldt, C., Kessler, V. & Persson, I. Structure of the hydrated, hydrolysed and solvated zirconium(iv) and hafnium(iv) ions in water and aprotic oxygen donor solvents. A crystallographic, EXAFS spectroscopic and large angle X-ray scattering study. *Dalton Trans.* **14**, 2142–2151 (2004).
8. Walther, C. et al. Investigation of polynuclear Zr(IV) hydroxide complexes by nanoelectrospray mass-spectrometry combined with XAFS. *Anal. Bioanal. Chem.* **388**, 409–431 (2007).
9. Cho, H.-R. et al. Combined LIBD and XAFS investigation of the formation and structure of Zr(IV) colloids. *Anal. Bioanal. Chem.* **383**, 28–40 (2005).
10. Rao, N., Holerca, M. N., Klein, M. L. & Pophristic, V. Computational study of the Zr^{4+} tetranuclear polymer, $[Zr_4(OH)_8(H_2O)_{16}]^{8+}$. *J. Phys. Chem. A* **111**, 11395–11399 (2007).
11. Gossard, A., Toquer, G., Grandjean, S. & Grandjean, A. Coupling between SAXS and Raman spectroscopy applied to the gelation of colloidal zirconium oxy-hydroxide systems. *J. Sol–Gel Sci. Technol.* **71**, 571–579 (2014).
12. Ely, M., Światowska, J., Seyeux, A., Zanna, S. & Marcus, P. Role of post-treatment in improved corrosion behavior of trivalent chromium protection (TCP) coating deposited on aluminum alloy 2024-T3. *J. Electrochem. Soc.* **164**, C276–C284 (2017).
13. Trinidad, C. et al. Effect of surface preparation treatments on copper enrichment on 2024 aluminium alloy surface. *Appl. Surf. Sci.* **560**, 149991 (2021).
14. Viroulaud, R. et al. Influence of surface pretreatments on the quality of trivalent chromium process coatings on aluminum alloy. *Appl. Surf. Sci.* **423**, 927–938 (2017).
15. Benninghoven, A., Niehuis, E., Greifendorf, D., van Leyen, D. & Lange, W. Analytical application of a high performance TOF-SIMS. In *Secondary Ion Mass Spectrometry SIMS* V. *Springer Series in Chemical Physics* Vol. 44 (eds Benninghoven, A. et al.) (Springer, Berlin, Heidelberg, 1986).
16. Wien, K. TOF-SIMS analysis of polymers. *Nucl. Instrum. Methods Phys. Res. B* **131**, 38–54 (1997).

17. Cristaudo, V. et al. A combined XPS/ToF-SIMS approach for the 3D compositional characterization of Zr-based conversion of galvanized steel. *Appl. Surf. Sci.* **562**, 150166 (2021).
18. Kraš, A., Kramar, D. & Milošev, I. Characterisation of the deposition and protection performance of Zr conversion coatings on steel and zinc substrates using the response surface methodology. (2024) (in the press).
19. Mujdrica Kim, M., Kapun, B., Tiringer, U., Šekularac, G. & Milošev, I. Protection of aluminium alloy 3003 in sodium chloride and simulated acid rain solutions by commercial conversion coatings containing Zr and Cr. *Coatings* **9**, 563 (2019).
20. Verdier, S., Delalande, S., van der Laak, N., Metson, J. & Dalard, F. Monochromatized x-ray photoelectron spectroscopy of the AM60 magnesium alloy surface after treatments in fluoride-based Ti and Zr solutions. *Surf. Interface Anal.* **37**, 509–516 (2005).
21. Šekularac, G., Kovač, J. & Milošev, I. Comparison of the electrochemical behaviour and self-sealing of zirconium conversion coatings applied on aluminium alloys of series 1xxx to 7xxx. *J. Electrochem. Soc.* **167**, 111506 (2020).
22. Barsoukov, E. & Macdonald, J. R. *Impedance Spectroscopy* (Wiley, Online Library 2005).
23. Campestrini, P., van Westing, E. P. M. & de Wit, J. H. W. Influence of surface preparation on performance of chromate conversion coatings on Alclad 2024 aluminium alloy: Part II: EIS investigation. *Electrochim. Acta* **46**, 2631–2647 (2001).
24. Otmacic Curkovic, H., Stupnisek-Lisac, E. & Takenouti, H. Electrochemical quartz crystal microbalance and electrochemical impedance spectroscopy study of copper corrosion inhibition by imidazoles. *Corros. Sci.* **51**, 2342–2348 (2009).
25. Abreu, C. M. et al. High frequency impedance spectroscopy study of passive films formed on AISI 316 stainless steel in alkaline medium. *J. Electroanal. Chem.* **572**, 335–345 (2004).
26. Andrade, C. et al. Electrochemical behaviour of steel rebars in concrete: influence of environmental factors and cement chemistry. *Electrochim. Acta* **46**, 3905–3912 (2001).
27. Özcan, M., Dehri, İ. & Erbil, M. EIS study of the effect of high levels of SO_2 on the corrosion of polyester-coated galvanised steel at different relative humidities. *Prog. Org. Coat.* **44**, 279–285 (2002).
28. Jiang, Q. et al. Electrochemical corrosion behavior of arc sprayed Al–Zn–Si–RE coatings on mild steel in 3.5% NaCl solution. *Trans. Nonferrous Met. Soc. China* **24**, 2713–2722 (2014).

Acknowledgements

The authors thank for the financial support provided by the Slovenian Research and Innovation Agency through the research core funding grant P2-0393 and project PR-09806. Région Ile-de-France is acknowledged for partial funding of the ToF-SIMS equipment.

Author contributions

A.K., I.M., A.S. and P.M. conceptualised the work. A.K. prepared the coatings and conducted EIS measurements and prepared the draft. A.S. conducted ToF-SIMS analysis. I.M. and P.M. supervised the work and edited and reviewed the final manuscript. All authors have read and agreed to the published version of the manuscript.

Competing interests

The authors declare no competing interests.

Additional information

Supplementary information The online version contains supplementary material available at https://doi.org/10.1038/s41529-024-00485-3.

Correspondence and requests for materials should be addressed to Ingrid Milošev or Philippe Marcus.